

# Design and measurement of a passive thrust magnetic bearing for a bearingless motor

Eric Severson\*, Astrid Røkke†, Robert Nilssen†, Tore Undeland†, and Ned Mohan\*

\*Department of Electrical and Computer Engineering  
University of Minnesota, Minneapolis, Minnesota 55455  
Email: sever212@umn.edu

†Department of Electric Power Engineering  
Norwegian University of Science and Technology, Trondheim, Norway  
Email: Astrid.Roekke@ntnu.no

**Abstract**—The design and construction of a permanent magnet thrust bearing for a bearingless motor is presented and a measurement technique is proposed to characterize the bearing. Optimal design of a bearingless motor requires the machine designer to be aware of the axial bearing's performance under simultaneous axial and radial displacement. A simple, low-cost test setup which requires only two single-axis load cells is proposed and evaluated to make these measurements on the magnetic bearing stator. The measurement data are found to be in reasonable agreement with finite element calculations and to satisfy Earnshaw's theorem, where the sum of stiffnesses in the three axes must be zero. The measurement technique displayed good test-retest reliability, with repeated radial force data having an average standard deviation of 2.1% for radial displacements greater than 0.5 mm and axial force data having a typical error of 0.9%.

**Index Terms**—magnetic bearing, bearingless motor, force measurement, magnetic levitation.

## I. INTRODUCTION

Bearingless electric machines are able to utilize the same iron to act as both a motor/generator and a magnetic bearing. These machines have been of recent interest for applications that require either high rotational speed or a clean environment where the rotor must be located in a sealed chamber [1]–[3]. Typically, bearingless machines are able to provide magnetic bearing functionality in the radial and tilting directions but rely on a separate bearing for axial support. Such machines are most efficient when the motor has a vertical shaft and gravitational forces are counteracted by this bearing which, for the applications listed above, is typically a passive magnetic bearing. Unlike axial mechanical bearings, axial magnetic bearing designs have considerable unstable radial forces and variation in the axial stiffness when the rotor becomes eccentric. When bearingless machines are powered down, their rotor is allowed to eccentrically rest upon "touchdown" or "backup" bearings in a position where such undesirable effects in the axial magnetic bearing can be highly pronounced.

For the bearingless machine designer, the force required to move the rotor from "rest" to a stable rotating position is a significant factor in determining the number of ampere-turns required for the suspension winding. Increasing the ampere-turns of the suspension winding decreases the space available

for the torque winding and thus decreases the torque density of the machine. It is therefore desirable that the design of the external magnetic bearing minimize the unstabilizing radial forces and necessary that changes in the radial and axial stiffness as a function of radial and axial displacement be accurately measured.

The design of an inexpensive, repulsive ring magnetic bearing utilizing neodymium magnets is considered for a bearingless ac homopolar machine. The radial unstabilizing force and changes in axial stiffness due to radial and axial displacement are explored through 3D finite element analysis, and a hardware prototype is constructed to validate the bearing performance with the proposed test method. The bearingless ac homopolar machine has been presented in [1], [4], [5] and is of interest to the authors as a vertical shaft machine for application in flywheel energy storage.

Several different measurement techniques for radial and axial force and stiffness values are found in the literature [2], [3], [6]–[15]. The only approach capable of measuring forces as a function of both axial and radial displacement uses an expensive three-axis load cell and an automated  $x$ - $y$ - $z$  cross table [6]. This work proposes an alternative technique which requires only two inexpensive single-axis load cells and a manual  $x$ - $y$  table. It is shown that this technique is able to measure the radial and axial forces of a magnetic thrust bearing over its entire range of operation.

In this paper: conventional techniques to measure radial and axial force/stiffness are reviewed; the design of a passive magnetic bearing for a bearingless ac homopolar machine through finite element analysis is presented; the proposed measurement technique is described; finally, a hardware prototype is constructed and used to characterize the designed magnetic bearing.

## II. CONVENTIONAL MEASUREMENT TECHNIQUES

### A. Measurement goals

Conventional approaches to radial and axial force and stiffness measurement are used in [2], [3], [6]–[15]. These measurements are made in test setups that include bearingless machines in [2], [3], [6]–[9]. In all of the aforementioned works, axial and radial force/stiffness are measured as a

function of axial and radial displacement, respectively, while the other dimension is maintained in its nominal position. In [13], the reduction in axial force at one particular radial displacement is given, but the effect of radial displacement is not investigated beyond this one point.

As mentioned earlier, for bearingless machines it is particularly important to be aware of forces from the permanent magnet bearing in positions where both dimensions are off-center, such as in a startup scenario. This work presents a technique to measure the radial and axial forces as a function of both radial and axial displacement.

### B. Measurement techniques

There are many different approaches to measuring the radial and axial forces. However, on a fundamental level, the approaches can be summarized as variations of the following:

- the rotor and stator are somehow mechanically displaced from each other and a device (such as a load cell) is used to measure the force along that direction for various displacements [3], [6], [7], [10], [13]–[15];
- a known force (i.e. a weight) is applied to the rotor along an axis and the displacement is measured for various forces; this will only work in cases where the magnetic bearing is stable in the displacement direction [3], [9], [10], [15].

There are also several different approaches to measuring the radial/axial stiffness, most of which can be summarized as variations of the following:

- extract the stiffness from the force data by fitting a linear regression line to the data as a function of displacement for small displacements [3], [6], [8], [10], [13], [15];
- excite the rotor with an impact hammer and observe the rotor’s frequency response [8], [14].

As an example, in [10] jewel bearings support each end of a flywheel axially, while two PM bearings provide radial stability to the horizontal axis. Radial forces are measured by removing the jewel bearing disk on one side, allowing it to be displaced radially, and adding weights to the shaft. Position is measured at two locations along the shaft. Axial forces are measured with a load cell placed in the jewel bearing assembly while the stators of the bearings are displaced axially. No combination of the two measurements are reported.

A common variation on the above techniques is used in [8] for measuring radial stiffness (axial stiffness is measured via the impact hammer test). Here, a consequent-pole bearingless motor is considered with a permanent magnet axial bearing. To measure the radial stiffness, the bearingless motor suspension force characteristic is first measured:  $k_f$  of the linearized magnetic bearing force model (1) is calculated by using the magnetic bearing controller to keep the rotor centered (fixing  $\delta = 0$  mm), applying a radial force to the rotor, and measuring the required suspension current,  $i_s$ .

$$F(\delta, i_s) = -k_s\delta + k_f i_s \quad (1)$$

Next, the controller is used to displace the rotor radially to a small value of  $\delta$ . When the rotor is in equilibrium,  $F(\delta, i_s) = 0$

and the radial stiffness is measured:  $k_s = k_f i_s / \delta$  with and without the permanent magnet bearing connected. While this is a very low-cost approach, there are two potential problems that must be carefully addressed on a per-device basis to ensure accurate results:

- the force model of (1) is typically only a linear approximation of the radial force’s dependence on displacement; it is therefore only accurate for sufficiently small values of  $\delta$  and it doesn’t account for axial displacement;
- as one of the same authors notes in [16], the radial suspension force of the bearingless motor can vary to a limited extent as a function of the rotor’s angular position, so if the rotor were to rotate between the time that the suspension force was characterized and the stiffness was measured, inaccurate results would be obtained.

Another variation is used in [15]. Here, the machine’s rotor is displaced to several small values of  $\delta$  by the controller. For each value, radial forces are applied to the rotor and the suspension current is measured while the controller keeps the displacement fixed. The bearing stiffness is approximated by dividing the difference in applied force for a given suspension current at two different displacements by the difference in displacement. Again, this suffers from the same potential inaccuracies as mentioned before. However, it is found that the method is sufficiently accurate for the device being considered in [15] under very small displacements.

Neither of the aforementioned variations are likely to provide acceptable radial stiffness measurements for large displacements in either the radial or axial direction and therefore don’t meet the goals of this paper. In [6], a force measurement procedure is described which should be capable of accurately measuring radial/axial forces as a function of both radial and axial displacement. Here, the stator is connected to a load cell capable of measuring forces in three dimensions. An automated 3D  $x$ - $y$ - $z$  cross-table is used to move the stator and rotor with respect to each other. While radial and axial force results are only reported for displacements along their respective axes, it appears that this setup could be used to accurately measure forces along both axes. However, such equipment is considerably more expensive than the equipment required for the measurement approach proposed in this work.

## III. DESIGN

A repulsive permanent magnet thrust bearing is designed using finite element analysis. The design goal is to minimize the radial unstabilizing forces and changes in the axial forces

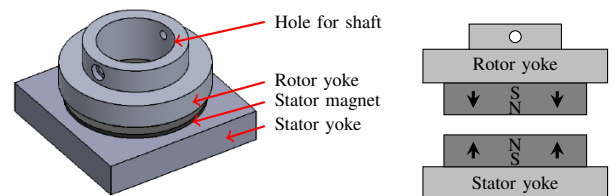


Fig. 1. Axial permanent magnet repulsion bearing

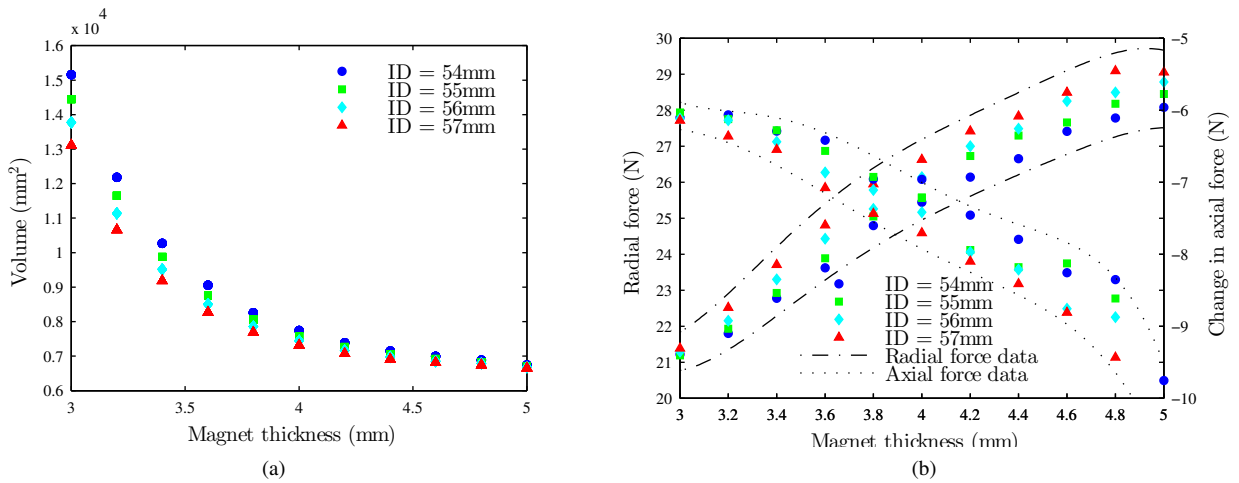


Fig. 2. 2D and 3D FEM results showing the effect of magnetic thickness and inner diameter on: (a) required magnet volume; (b) magnetic bearing radial and axial forces when the rotor is resting on its touch down bearings ( $\delta = 1.5$  mm).

TABLE I  
MAGNETIC BEARING DESIGN

Magnet thickness	3.4 mm
Inner diameter	55 mm
Outer diameter	82 mm
Magnet material	NdFeB Grade N42
Remanent flux density	1.28 T
Coercivity	915 kA/m

when the rotor is fully eccentric (resting upon its touchdown bearings) and minimize the design cost by minimizing the magnet volume. The simple repulsive ring magnetic bearing design depicted in Fig. 1 is chosen, which requires only two pieces of magnetic material and two back yokes. The bearing stator consists of an axially magnetized ring permanent magnet glued to an aluminum yoke. The rotor consists of an axially magnetized ring magnet glued to an aluminum sleeve which is secured to the bottom of the bearingless motor's rotor shaft.

The design of the bearing is explored through 2D and 3D finite element simulations in Fig. 2. The rotor weight, desired airgap, and magnet material properties are assumed constant. For various acceptable magnet thicknesses and inner diameters, 2D finite element analysis is performed to find the required magnetic outer diameter to support the rotor weight with the desired airgap. The magnetic volume is then calculated from the magnet dimensions and 3D finite element analysis is conducted to determine the radial unstabilizing force and changes in the axial supporting force when the bearing is fully eccentric (that is, when the bearingless motor's rotor is resting on the touchdown bearings). The final design is specified in Table I and additional finite element results are considered later, in Fig. 5.

#### IV. PROPOSED MEASUREMENT TECHNIQUE

To characterize the permanent magnet bearing, the test stand depicted in Fig. 3 and Fig. 4 was built. The rotor is fixed

radially but is free to move axially. This is accomplished by mounting two brass sliding bearings on the housing of the homopolar bearing. The permanent magnet bearing stator is restricted axially and movements in the radial direction are controlled by a manual  $x$ - $y$  cross-table. The connection to the cross-table is through single-axis load cells. An " $x$ " and a " $y$ " load cell are each connected to a side of the bearing stator through inline ball-joint linkages. The ball-joint linkages are used instead of bolts to decrease any cross-talk between the sensors, as they will only support forces along their axes. The permanent magnet bearing stator rests axially against eight ball transfer units which have been installed in the crosspiece and are shown in Fig. 3c. The ball transfer units prevent friction between the bearing stator and the crosspiece that could interfere with radial force measurement. The radial force sensors are also mounted to this crosspiece and the entire apparatus is centered on top of another single-axis load cell for axial force measurements.

The rotor can be displaced axially by placing weights upon it (see the basket on the top of Fig. 3a) while the stator can be displaced radially by adjusting the  $x$ - $y$  cross-table. Since the brass sliding bearings have some axial friction, the value of the weights added to the top of the rotor are ignored and instead the axial load cell is used to measure the axial force that the bearing provides. The rotor's axial displacement is measured via a dial indicator while the  $x$ - $y$  cross-table is able to accurately position the stator to within 0.025 mm.

All measurements are taken with the bearingless homopolar machine completely powered down.

#### V. RESULTS

Radial and axial force measurements are shown in Fig. 5. The airgap between the permanent magnet bearing and stator was measured at being 2.55 mm nominally, which, as can be seen in Fig. 5a, matches the finite element simulations. The radial and axial stiffness values about the nominal positions were calculated from linear regression lines fitted to the data

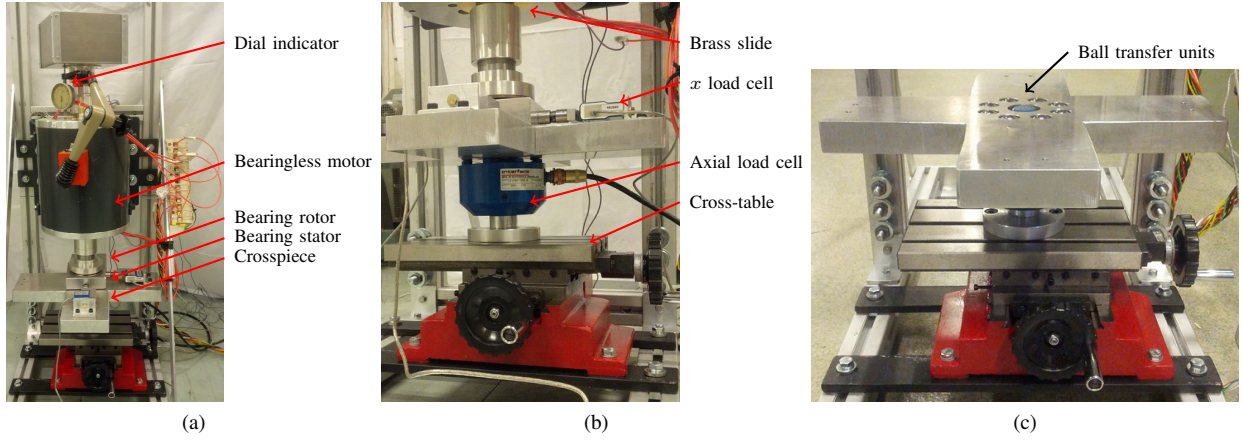


Fig. 3. Photographs of (a) the full test stand; (b) the measurement apparatus; and (c) the bottom of the test stand with the permanent magnet bearing and radial load cells removed.

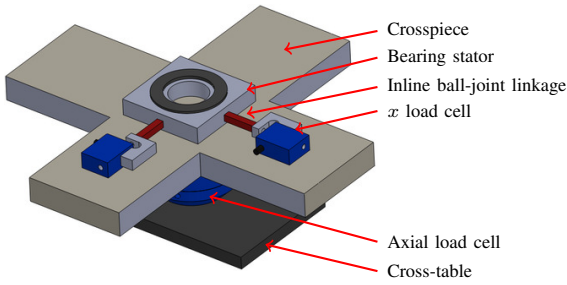


Fig. 4. Drawing of measurement apparatus

TABLE II  
STIFFNESS RESULTS

Parameter <sup>a</sup>	Measured	FEM Result
Radial Stiffness (N/mm)	16.8	16.2
Axial Stiffness (N/mm)	33.3	32.4

<sup>a</sup>All stiffness values are reported about the nominal position and are taken as the slope of the regression lines shown in Fig. 5

and shown in Fig. 5a and b. These stiffness values are given in Table II. Note that the measured radial stiffness value is approximately 4% greater than the FEM calculation and the measured axial stiffness is approximately 3% greater than the FEM calculation. Earnshaw's theorem predicts that for an axially symmetric magnetic bearing without iron, the axial stiffness should be twice the radial stiffness [17], [18]. The finite element results satisfy this exactly and the small discrepancy in the measured results can be explained by measurement uncertainty, as discussed later.

The radial and axial force measurements as a function of both radial and axial displacement are shown in Fig. 2c and d. The range of radial displacement is selected to be -1.5 mm to 1.5 mm to include the displacement when the bearingless ac homopolar machine is powered down and the shaft is resting upon the touchdown bearings. Fig. 2e and f show finite element analysis results for the same displacements.

### A. Repeatability

To assess the repeatability of the radial force measurements, the radial force data shown in Fig. 5b was collected eight times for each radial offset. The standard deviation in measurement data at each radial displacement is calculated. The average of these values is 0.4 N and all standard deviations are within 0.1 N of this. For radial displacements greater than 0.5 mm, the average standard deviation was 2.1% of the average force measured.

Assessing the repeatability of the axial force measurements is more challenging. Since the brass slides exert a frictional force on the rotor shaft, both the axial displacement and axial force differed between measurements for the same weight being placed upon the shaft. Therefore, it is not possible to compare force variation for the same axial displacement. Instead, it was observed from the finite element simulations that a quadratic polynomial accurately fit the axial force dependence upon axial displacement. The measured data shown in Fig. 5a were fit to a quadratic polynomial using the least squares method and the force difference between each measured data point and the value predicted by the polynomial was calculated and normalized by the value predicted by the polynomial. The average of the normalized error magnitudes is 0.9%.

The repeatability for both radial and axial forces are considered to be very good and any significant measurement error must be due to a systemic bias.

### B. Systemic errors

There were two primary sources for systemic bias error observed in the measurements. The first is that the airgap between the permanent magnet bearing and stator was not completely parallel. It was measured at being 2.55 mm nominally and, despite efforts to mount the two surfaces perfectly parallel, there was a deviation of approximately 0.05 mm measured. Finite element simulations results showed that this could lead to a maximum difference in force measurements of 0.9 N over all values of axial and radial displacements tested, which was

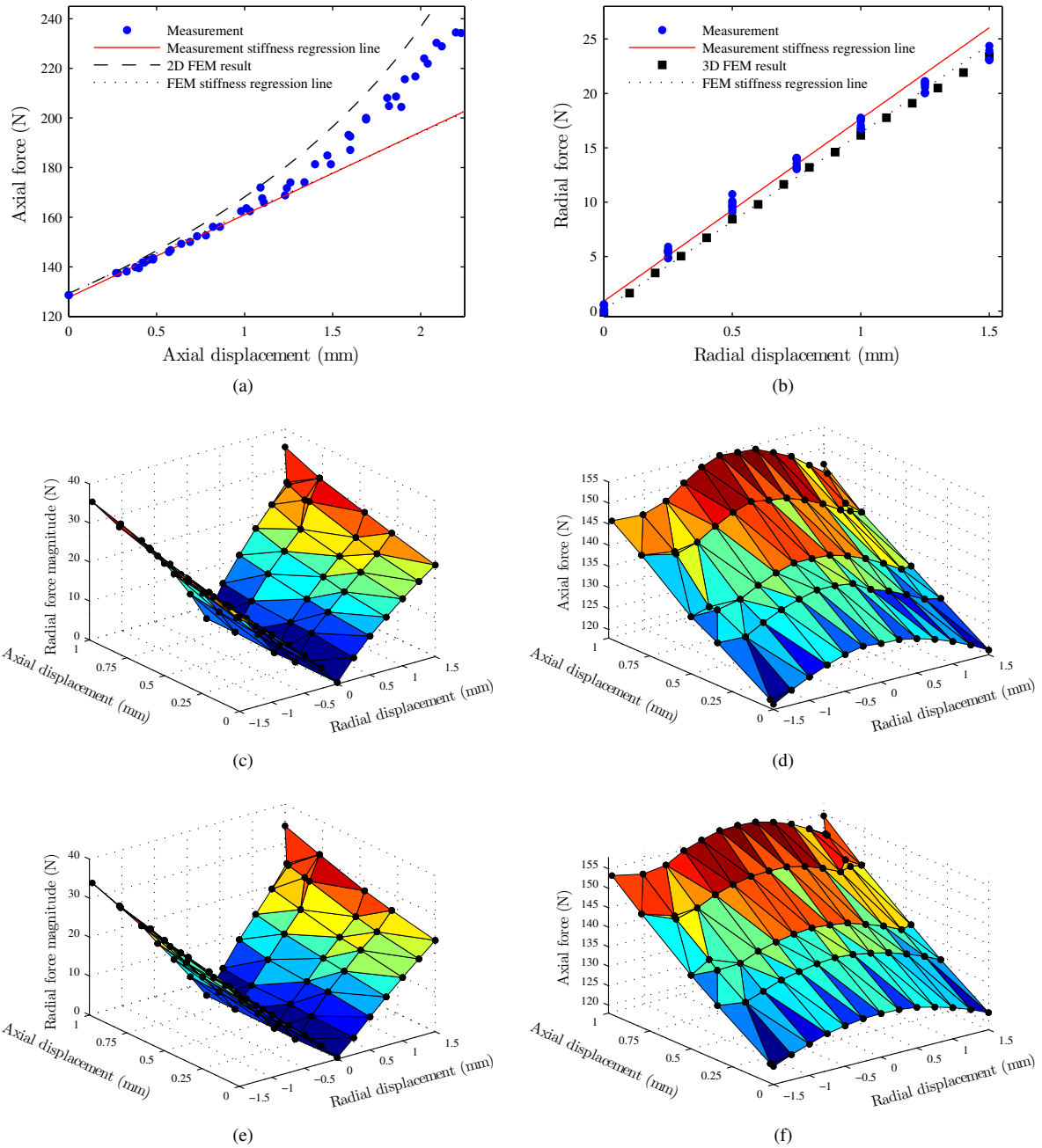


Fig. 5. (a) Axial force measurements when the rotor is centered; (b) radial force measurements when the airgap is at its nominal value; (c) radial force measurements under both axial and radial displacement; (d) axial force measurements under both axial and radial displacement; (e) 3D FEM results for radial forces and (f) 3D FEM results for axial forces under the same displacements as in c) and d); note that positive values of axial displacement indicate a smaller airgap.

deemed acceptable. The finite element simulations predicted that for each value of axial displacement, the maximum force difference between the parallel and non-parallel cases would occur for small radial displacements, which possibly accounts for the non-zero radial forces at zero radial displacement shown in Fig. 5.

The second source for measurement error was noticeable cross-coupling between the  $x$  and  $y$  load cells, despite the

ball-joint linkages. All data was collected by keeping the  $y$ -axis in its nominal position and displacing the  $x$ -axis. Ideally, the  $y$ -axis load cell would always read 0 N. Instead, as can be seen in Fig. 6, the  $y$ -axis had a substantial offset and varied as a function of  $x$ -axis displacement. In addition to this, Fig. 6 shows that the  $x$ -axis load cell also had a substantial offset. To correct for the offset, a regression line was fitted over all the  $x$ -axis data points. Ideally, the  $x$ -axis data should be perfectly

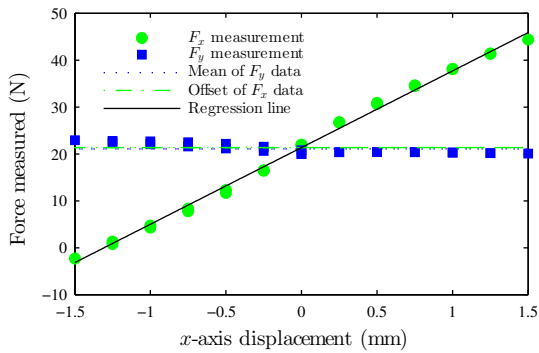


Fig. 6. Example set of measured data with 2.55 mm airgap

symmetric about the center point ( $x = 0$  mm). For this reason, the offset of the linear regression line was treated as the offset of the data. This procedure was applied to all of the radial data measurements. It is interesting to note that the average value of the  $y$ -axis force data (21.1 N in Fig. 6) is approximately equal to the determined offset in the  $x$ -axis data (21.3 N in Fig. 6). This implies that the effect of the airgap not being perfectly parallel is minimal.

Note that the data from the  $y$ -axis load cell was not used for any results other than to investigate cross-coupling. All of the presented force measurements in Fig. 5 were taken from only two single-axis load cells: one axial load cell and one radial load cell. Initially, the test apparatus was designed to utilize five single-axis load cells to enable differential  $x$ - and  $y$ -axis measurements. The expectation was that such measurements would lead to more accurate results. However, the opposite was true. Misalignment with the additional sensors caused tension along both the  $x$ - and  $y$ -axis which caused cross-axis coupling in the force measurement.

## VI. CONCLUSION

A simple axial repulsion magnetic bearing was designed using the finite element method, where the design requirements unique to the application of a bearingless motor were considered. A hardware prototype was constructed and measurements taken with a proposed measurement technique were found to be in agreement with finite element calculations and satisfied the stiffness requirements for an axially symmetric magnetic bearing predicted by Earnshaw's theorem.

An inexpensive measurement technique was proposed for measuring the radial and axial force of the designed magnetic bearing over the entire radial and axial range of operation. High repeatability characteristics were observed in the radial and axial directions and it is concluded that this measurement technique is a viable alternative to techniques that require significantly more expensive measurement equipment.

## ACKNOWLEDGMENT

This research is partly supported by the Norwegian Centre for International Cooperation in Education (SIU) and was carried out in part using computing resources at the University

of Minnesota Supercomputing Institute. This material is based upon work supported by the National Science Foundation Graduate Research Fellowship Program under Grant No. 00006595.

## REFERENCES

- [1] J. Asama, R. Natsume, H. Fukuhara, T. Oiwa, and A. Chiba, "Optimal suspension winding configuration in a homo-polar bearingless motor," *Magnetics, IEEE Transactions on*, vol. 48, no. 11, pp. 2973–2976, nov. 2012.
- [2] B. Warberger, R. Kaelin, T. Nussbaumer, and J. Kolar, "50-/2500-w bearingless motor for high-purity pharmaceutical mixing," *Industrial Electronics, IEEE Transactions on*, vol. 59, no. 5, pp. 2236–2247, 2012.
- [3] P. Karutz, T. Nussbaumer, W. Gruber, and J. Kolar, "Novel magnetically levitated two-level motor," *Mechatronics, IEEE/ASME Transactions on*, vol. 13, no. 6, pp. 658–668, dec. 2008.
- [4] O. Ichikawa, A. Chiba, and T. Fukao, "Inherently decoupled magnetic suspension in homopolar-type bearingless motors," *Industry Applications, IEEE Transactions on*, vol. 37, no. 6, pp. 1668–1674, nov/dec 2001.
- [5] E. Severson, R. Nilssen, T. Undeland, and N. Mohan, "Analysis of the bearingless ac homopolar motor," in *International Conference on Electrical Machines (ICEM)*, 2012., Sep. 2012, pp. 568–574.
- [6] W. Gruber, H. Grabner, S. Silber, and W. Amrhein, "Design of a brushless permanent magnet synchronous drive with a merely passively suspended rotor," in *Power Electronics, Electrical Drives, Automation and Motion (SPEEDAM), International Symposium on*, 2012, pp. 597–602.
- [7] H. Grabner, W. Amrhein, S. Silber, and W. Gruber, "Nonlinear feedback control of a bearingless brushless dc motor," *Mechatronics, IEEE/ASME Transactions on*, vol. 15, no. 1, pp. 40–47, Feb.
- [8] J. Asama, T. Asami, T. Imakawa, A. Chiba, A. Nakajima, and M. Rahman, "Effects of permanent-magnet passive magnetic bearing on a two-axis actively regulated low-speed bearingless motor," *IEEE Transactions on Energy Conversion*, vol. 26, no. 1, pp. 46–54, 2011.
- [9] F. Wang and L. Xu, "Calculation and measurement of radial and axial forces for a bearingless pm dc motor," in *Industry Applications Conference, 2000. Conference Record of the 2000 IEEE*, vol. 1, pp. 249–252 vol.1.
- [10] M. Siebert, B. Ebihara, R. Jansen, R. Fusaro, A. Kascak, and A. Kenny, "A passive magnetic bearing flywheel," in *Proceedings of the Intersociety Energy Conversion Engineering Conference*, Feb. 2002, pp. 125–132.
- [11] T. Ohji, S. Mukhopadhyay, M. Iwahara, and S. Yamada, "Permanent magnet bearings for horizontal- and vertical-shaft machines: A comparative study," *Journal of Applied Physics*, vol. 85, no. 8, pp. 4648–4650, Apr 1999.
- [12] R. De Andrade Jr., G. Sotelo, A. Ferreira, L. Rolim, J. Da Silva Neto, R. Stephan, W. Suemitsu, and R. Nicolosky, "Flywheel energy storage system description and tests," *IEEE Transactions on Applied Superconductivity*, vol. 17, no. 2, pp. 2154–2157, 2007.
- [13] G. Sotelo, R. De Andrade Jr., and A. Ferreira, "Magnetic bearing sets for a flywheel system," *IEEE Transactions on Applied Superconductivity*, vol. 17, no. 2, pp. 2150–2153, 2007.
- [14] R. Stephan, R. De Andrade Jr., G. Dos Santos, M. Neves, and R. Nicolosky, "Levitation force and stability of superconducting linear bearings using ndfeb and ferrite magnets," *Physica C: Superconductivity and its Applications*, vol. 386, pp. 490–494, 2003.
- [15] M. Autila, E. Lantto, and A. Arkkio, "Determination of forces and linearized parameters of radial active magnetic bearings by finite element technique," *Magnetics, IEEE Transactions on*, vol. 34, no. 3, pp. 684–694, May 1998.
- [16] J. Amemiya, A. Chiba, D. Dorrell, and T. Fukao, "Basic characteristics of a consequent-pole-type bearingless motor," *Magnetics, IEEE Transactions on*, vol. 41, no. 1, pp. 82–89, jan. 2005.
- [17] S. Earnshaw, "On the nature of the molecular forces which regulate the constitution of the luminiferous ether," *Trans. Camb. Phil. Soc.*, vol. 7, pp. 97–112, 1842.
- [18] J. Delamare, E. Rulliere, and J. Yonnet, "Classification and synthesis of permanent magnet bearing configurations," *IEEE Transactions on Magnetics*, vol. 31, no. 6 pt 2, pp. 4190–4192, 1995.